J|A|C|S ARTICLES

Published on Web 10/20/2010

QM/MD Simulation of SWNT Nucleation on Transition-Metal Carbide Nanoparticles

Alister J. Page,[†] Honami Yamane,[†] Yasuhito Ohta,[‡] Stephan Irle,*[,§] and Keiji Morokuma*[,†,||]

Fukui Institute for Fundamental Chemistry, Kyoto University, Kyoto 606-8103, Japan, Department of Chemistry, Nara Women's University, Nara 630-8605, Japan, Institute for Advanced Research and Department of Chemistry, Nagoya University, Nagoya 464-8602, Japan, and Cherry L. Emerson Center for Scientific Computation and Department of Chemistry, Emory University, Atlanta, Georgia 30322

Received July 24, 2010; E-mail: sirle@iar.nagoya-u.ac.jp (S.I.); morokuma@fukui.kyoto-u.ac.jp (K.M.)

Abstract: The mechanism and kinetics of single-walled carbon nanotube (SWNT) nucleation from Fe- and Ni-carbide nanoparticle precursors have been investigated using quantum chemical molecular dynamics (QM/MD) methods. The dependence of the nucleation mechanism and its kinetics on environmental factors, including temperature and metal-carbide carbon concentration, has also been elucidated. It was observed that SWNT nucleation occurred via three distinct stages, viz. the precipitation of the carbon from the metal-carbide, the formation of a "surface/subsurface" carbide intermediate species, and finally the formation of a nascent sp^2-hybidrized carbon structure supported by the metal catalyst. The SWNT cap nucleation mechanism itself was unaffected by carbon concentration and/or temperature. However, the kinetics of SWNT nucleation exhibited distinct dependences on these same factors. In particular, SWNT nucleation from Ni_xC_y nanoparticles proceeded more favorably compared to nucleation from Fe_xC_y nanoparticles. Although SWNT nucleation from Fe_xC_y and Ni_xC_y nanoparticle precursors occurred via an identical route, the ultimate outcomes of these processes also differed substantially. Explicitly, the Ni_x-supported sp^2-hybridized carbon structures tended to encapsulate the catalyst particle itself, whereas the Fe_x-supported structures tended to form isolated SWNT cap structures on the catalyst surface. These differences in SWNT nucleation kinetics were attributed directly to the relative strengths of the metal−carbon interaction, which also dictates the precipitation of carbon from the nanoparticle bulk and the longevity of the resultant surface/subsurface carbide species. The stability of the surface/subsurface carbide was also influenced by the phase of the nanoparticle itself. The observations agree well with experimentally available data for SWNT growth on iron and nickel catalyst particles.

1. Introduction

The discovery of carbon nanotubes, and subsequently single-walled carbon nanotubes[1−3] (SWNTs), heralded a new era of science and technology at the molecular level. In the intervening years, the synthesis of SWNTs from transition metal catalysts has become a routine process at the industrial and commercial scale. Significant efforts toward understanding exactly how SWNT nucleation and growth occurs have been made during this time. Consequently, models of SWNT nucleation and growth derived from experimental and theoretical investigations have converged toward each other in recent years. A relatively unified picture of how SWNT nucleation and growth occur, based on the vapor−liquid−solid (VLS) mechanism, therefore now exists (see, for example, refs 4−6 and references therein). However, absolute control over tube diameter and (*n*,*m*) chirality during synthesis remains elusive.

One aspect of SWNT nucleation over which experimental and theoretical data do not currently agree is the existence of the transition metal-carbide precursor assumed in the VLS model.[7] A number of experimental investigations reported in the literature show the existence of (for example) Fe_3C, Ni_3C, *etc.* nanoparticles prior to SWNT nucleation[8−11] or during periods of catalytic activity.[12] On the other hand, purely metallic catalyst particles have also been observed to actively grow SWNTs in both Fe[13] and Ni[14] cases. Despite this, the existence of bulk carbide is now commonly assumed in the literature. To our knowledge, however, the stability of bulk carbide nanoparticles at experimental SWNT growth temperatures and over lab

[†] Kyoto University.
[‡] Nara Women's University.
[§] Nagoya University.
[||] Emory University.

(1) Iijima, S. *Nature* **1991**, *354*, 56–58.
(2) Iijima, S.; Ichihashi, T. *Nature* **1993**, *363*, 603–605.
(3) Bethune, D. S.; Klang, C. H.; de Vries, M. S.; Gorman, G.; Savoy, R.; Vazquez, J.; Beyers, R. *Nature* **1993**, *363*, 605–607.
(4) Harris, P. J. F. *Carbon* **2007**, *45*, 229–239.
(5) Gavillet, J.; Thibault, J.; Stephan, O.; Amara, H.; Loiseau, A.; Ch., B.; Gaspard, J.-P.; Ducastelle, F. *J. Nanosci. Nanotechnol.* **2004**, *4*, 346–359.
(6) Irle, S.; Ohta, Y.; Okamoto, Y.; Page, A. J.; Wang, Y.; Morokuma, K. *Nano Res.* **2009**, *2*, 755–767.
(7) Jiang, K.; Feng, C.; Liu, K.; Fan, S. *J. Nanosci. Nanotechnol.* **2007**, *7*, 1494–1504.

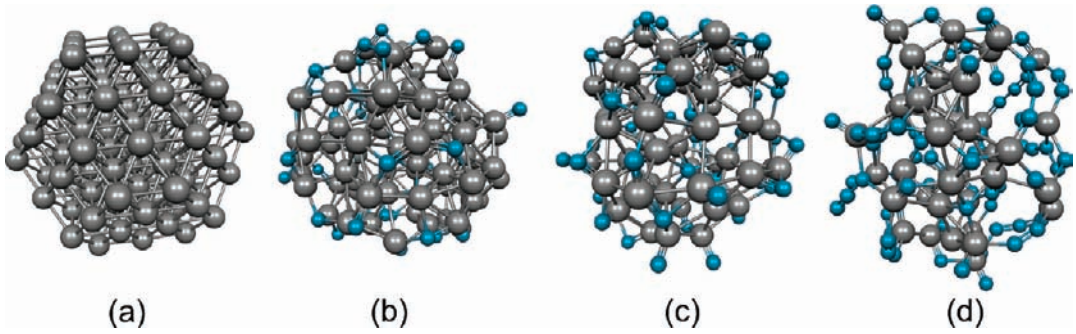

Figure 1. Optimized geometries of the (a) Ni_{116}, (b) $Ni_{77}C_{39}$, (c) $Ni_{58}C_{58}$, and (d) $Ni_{39}C_{77}$ model systems. Gray and cyan spheres represent Ni and C atoms, respectively.

time scales has not yet been demonstrated theoretically. Instead, prevalent theoretical models of such dissolution of carbon into relevant transition metals suggest that the most energetically favorable carbide structure is a "subsurface" carbide (i.e., one in which carbon preferentially resides at, or near, the metal surface, as opposed to the bulk).[15−18] Recent experimental results concerning the solubility of carbon in iron nanoparticles also lends weight to this idea.[19] It has even been shown that the formation of a carbide phase is not a necessary prerequisite for SWNT nucleation on Fe_{38} nanoparticles.[20] Nevertheless, very few investigations into the existence and stability of transition metal-carbide nanostructures have been performed from a quantum mechanical (QM) perspective.[21,22]

An atomistic mechanism of Fe_{38}-catalyzed SWNT nucleation has been elucidated using QM molecular dynamics (MD) techniques in a recent investigation.[20] This mechanism essentially consists of three distinct steps, and the dynamics of carbon structure growth and transformation resembles closely the formation mechanism of fullerenes.[23] First, carbon atoms adsorbed on the catalyst nanoparticle surface diffuse across the surface and coalesce, forming extended polyyne chains; these polyyne chains themselves then coalesce, producing "Y"-shaped junctions and ultimately a five-membered ring (the SWNT "seed"). The second stage in the SWNT nucleation mechanism consists of adjacent polyyne chains bonded to this five-membered carbon ring isomerizing, yielding further formation of five-, six- and seven-membered rings. No discernible preference is observed (i.e., with respect to the type of rings added to the sp^2-hybridized carbon network) at this stage of the mechanism. The final stage of the SWNT mechanism consists of the conversion of five-membered rings to six-membered rings assisted by the interaction of short-lived polyyne chains.

In this work, we applied QM/MD investigations into the mechanisms of SWNT nucleation and growth from iron- and nickel-carbide nanoparticle precursors. As in our previous studies of SWNT nucleation and growth on pristine iron and nickel nanoparticles,[20,24] we employed the self-consistent charge density-functional tight-binding (SCC-DFTB/MD)[25] method, in conjunction with model Fe_xC_y and Ni_xC_y "amorphous" nanoparticle precursors. In this study we address the atomistic mechanism of metal−carbon phase separation, the cap nucleation, and sidewall growth mechanisms, and we also address the outstanding questions regarding the stability and existence of transition metal-carbide precursors that precede SWNT nucleation and growth. The effects of pertinent environmental factors, including temperature and metal-carbide carbon concentration,[26] on the mechanism and kinetics of SWNT nucleation, as well as the stability of the iron- and nickel-carbide phase, are also focused upon in the present study. Our atomic-scale simulations provide valuable insight into the open question of how a growing SWNT affects the stability of the metal-carbide phase.

2. Computational Methodology

2.1. Fe_xC_y and Ni_xC_y Model Systems. SWNT nucleation was simulated with the existence of a metal-carbide precursor assumed *a priori*. Initially, Ni_{116} and Fe_{116} nanoparticles were constructed from the respective bulk fcc phase. These nanoparticles exhibited diameters of 1.26 and 1.29 nm, respectively, and are therefore consistent with commonly produced SWNT diameter distributions.[27,28] Individual metal atoms, selected at random, were then replaced with carbon atoms. The metal-carbide model system is depicted in Figure 1 for the case of Ni. In the Ni- and Fe-carbide bulk, carbon occupies the octahedral and tetrahedral sites, respectively. Therefore, the carbide structures produced here *via* the

(8) Lin, M.; Ying Tan, J. P.; Boothroyd, C.; Loh, K. P.; Tok, E. S.; Foo, Y.-L. *Nano Lett.* **2006**, *6*, 449–452.
(9) Yoshida, H.; Takeda, S.; Uchiyama, T.; Kohno, H.; Homma, Y. *Nano Lett.* **2008**, *8*, 2082–2086.
(10) Zhang, Y.; Li, Y.; Kim, W.; Wang, D.; Dai, H. *Appl. Phys. A: Mater. Sci. Process.* **2002**, *74*, 325–328.
(11) Zhu, H.; Suenaga, K.; Hashimoto, A.; Urita, K.; Hata, K.; Iijima, S. *Small* **2005**, *1*, 1180–1183.
(12) Stolojan, V.; Tison, Y.; Chen, G. Y.; Silva, R. *Nano Lett.* **2006**, *6*, 1837–1841.
(13) Anisimov, A. S.; Nasibuling, A. G.; Jiang, H.; Launois, P.; Cambedouzou, J.; Shandakov, S. D.; Kauppinen, E. I. *Carbon* **2010**, *48*, 380–388.
(14) Hofmann, S.; et al. *Nano Lett.* **2007**, *7*, 602–608.
(15) Amara, H.; Bichara, C.; Ducastelle, F. *Phys. Rev. B* **2006**, *73*, 113404.
(16) Amara, H.; Bichara, C.; Ducastelle, F. *Phys. Rev. Lett.* **2008**, *100*, 056105.
(17) Amara, H.; Bichara, C.; Ducastelle, F. *J. Nanosci. Nanotechnol.* **2008**, *8*, 6099–6104.
(18) Amara, H.; Roussel, J. M.; Bichara, C.; Gaspard, J. P.; Ducastelle, F. *Phys. Rev. B* **2009**, *79*, 014109.
(19) Harutyunyan, A. R.; Awasthi, N.; Jiang, A.; Setyawan, W.; Mora, E.; Tokune, T.; Bolton, K.; Curtarolo, S. *Phys. Rev. Lett.* **2008**, *100*, 195502.
(20) Ohta, Y.; Okamoto, Y.; Page, A. J.; Irle, S.; Morokuma, K. *ACS Nano* **2009**, *3*, 3413–3420 (doi: 10.1021/nn900784f).
(21) Raty, J.-Y.; Gygi, F.; Galli, G. *Phys. Rev. Lett.* **2005**, *95*, 096103.
(22) Zhu, W.; Börjesson, A.; Bolton, K. *Carbon* **2010**, *48*, 470–478.
(23) Irle, S.; Zheng, G.; Wang, Z.; Morokuma, K. *J. Phys. Chem. B* **2006**, *110*, 14531–14545.
(24) Page, A. J.; Ohta, Y.; Irle, S.; Morokuma, K. *Acc. Chem. Res.* **2010**, ASAP paper (doi: 10.1021/ar100064g).
(25) Elstner, M.; Porezag, D.; Jungnickel, G.; Elsner, J.; Haugk, M.; Frauenheim, T.; Suhai, S.; Seifert, G. *Phys. Rev. B* **1998**, *58*, 7260.
(26) Neyts, E.; Shibuta, Y.; Bogaerts, A. *Chem. Phys. Lett.* **2010**, *488*, 202–205.
(27) Bachilo, S. M.; Balzano, L.; Herrera, J. E.; Pompeo, F.; Resasco, D. E.; Weisman, R. B. *J. Am. Chem. Soc.* **2003**, *125*, 11186–11187.
(28) Lolli, G.; Zhang, L.; Balzano, L.; Sakulchaicharoen, N.; Tan, Y.; Resasco, D. E. *J. Phys. Chem. B* **2006**, *110*, 2108–2115.

random replacement of metal atoms are generally expected to be less stable structures. Nevertheless, it has previously been established[20] that annealing pristine metal nanoparticles at high temperature and/or low pressure yields an almost instantaneous loss of crystalline structure. We anticipate this also to be the case in the present context. The metal-carbide nanoparticles created in this manner resembled amorphous metal−carbon phases, as opposed to bulk crystalline structures. Nevertheless, recent experimental[19] and theoretical[29] investigations suggest that such amorphous species do indeed exist prior to SWNT nucleation, particularly for 'pure-VLS' conditions (such as those observed during arc-discharge experiments). The results from recent MD simulations[26] have shown that it is necessary to consider the effect of carbon concentration (within the nanoparticle precursor) on SWNT nucleation and growth. To this end, differing amounts of carbon substitution were considered in order to ascertain the effect of the metal-carbide carbon concentration on the mechanism and kinetics of Ni- and Fe-catalyzed SWNT nucleation. In particular, 39, 58, and 77 metal atoms (i.e., 33%, 50%, 66% of all metal atoms) were replaced with carbon in both Ni_{116} and Fe_{116}, yielding $Ni_{77}C_{39}$/$Fe_{77}C_{39}$, $Ni_{58}C_{58}$/$Fe_{58}C_{58}$, and $Ni_{39}C_{77}$/$Fe_{39}C_{77}$ nanoparticles. A carbon concentration of 66% is unrealistic but has been employed here for the purposes of comparison. To ascertain the effects of temperature on the Fe- and Ni-catalyzed SWNT nucleation mechanism and kinetics, SCC-DFTB/MD simulations were performed using T_n values of 800, 1400, and 2000 K. While temperatures of 800 and 1400 K are typical of chemical vapor deposition (CVD) experiments, the higher temperature of 2000 K is more relevant to laser ablation or arc-discharge techniques. Each combination of metal type, carbon concentration, and temperature was replicated 10 times, resulting in a total of 180 MD trajectories. These trajectories are denoted as M_xC_y@*T*-*N*, where M denotes the metal employed, *x*/*y* denote the number of atoms, *T* is the simulation temperature in K, and *N* denotes the trajectory number (1−10). For each trajectory, SWNT nucleation was simulated using SCC-DFTB/MD for 300 ps.

The phase of the Fe_xC_y and Ni_xC_y nanoparticles has been estimated using the Lindemann Index, δ,[30]

$$\delta = \frac{1}{N(N-1)} \sum_{i<j} \frac{\sqrt{\langle r_{ij}^2 \rangle_T - \langle r_{ij} \rangle_T^2}}{\langle r_{ij} \rangle_T}$$

where *N* is the number of atoms, r_{ij} is the instantaneous distance between atoms *i* and *j*, and T denotes thermal averaging at temperature *T*. All δ values reported in this work have been calculated ignoring all carbon atoms within the nanoparticle (i.e., δ is effectively a "metal-only" value) have been averaged over the 10 trajectories (for each combination of carbon concentration and simulation temperature).

2.2. Molecular Dynamics. SWNT nucleation has been investigated using QM/MD methods. The quantum mechanical potential was calculated at each MD iteration using the SCC-DFTB method.[25] Parameters developed previously in our group[31] for carbon, iron, and nickel were employed. The *p* orbitals of carbon and the *d* orbitals of nickel/iron were therefore included in this description of electronic structure. A finite electronic temperature[32,33] of 10 000 K was enforced on the wave function of the Ni_xC_y and Fe_xC_y model systems. The occupation of each molecular orbital was therefore described by a Fermi−Dirac distribution function of that orbital's energy. All molecular orbital occupations could therefore vary continuously over [0,2]. In reality however, such fractional occupations are observed only for those orbitals at or near the Fermi level. Such an "electron-smearing" approach has been used and validated by us in a previous investigation of SWNT nucleation.[20] Following the optimization of the Ni_xC_y and Fe_xC_y model systems' geometries to local minima, the structures were annealed at constant temperature (i.e., NVT-MD). The initial velocity of each atom was calculated using a Boltzmann distribution at the respective nuclear temperature and was, therefore, randomly constructed. This ensured that each individual trajectory was statistically independent. The Newtonian equations of motion were integrated numerically using the Velocity-Verlet algorithm[34] with a discrete time step of 1 fs, and the nuclear temperature (T_n) was maintained using a Nosé−Hoover chain thermostat[35] coupled to the degrees of freedom of the system.

3. Results and Discussion

3.1. SWNT Nucleation from Ni_xC_y Nanoparticles. We begin by considering SWNT nucleation from Ni_xC_y nanoparticle precursors. Upon constant temperature thermal annealing of these species, it was observed for all choices of carbon concentration and simulation temperature that carbon atoms precipitated from within the carbide nanoparticle to its surface almost immediately (i.e., within several hundred picoseconds). The transition between the metal-carbide phase and a segregated metal−carbon system therefore took place very rapidly according to these simulations. The dynamics of this transition and the stability of the metal-carbide and subsurface/surface carbide will be discussed at greater length in subsequent sections. Instead, we discuss here the explicit mechanism of SWNT nucleation from Ni_xC_y nanoparticle precursors.

The mechanism of SWNT nucleation from Ni_xC_y nanoparticle precursors observed in this work is depicted in Figure 2. This figure corresponds to Trajectories $Ni_{77}C_{39}$@1400K-5 and $Ni_{58}C_{58}$@1400K-3, which typify the dynamics observed under the respective simulation conditions. Figures depicting SWNT nucleation from Ni_xC_y nanoparticle precursors at 800 and 2000 K are available in the Supporting Information. Precipitation of carbon in both trajectories proceeded rapidly, resulting in the formation of a surface carbide structure within *ca*. 5 and 15 ps, respectively. Moreover, the structure of this surface carbide itself changed quickly, from isolated carbon atoms residing on the catalyst surface to C_n ($n \geq 3$) chains bound to the catalyst surface. This transformation was mediated by the surface diffusion of the carbon atoms themselves, which, although essentially random, was assisted by the weakness of the Ni−C interaction. It is noted at this juncture that the strength of this catalyst−carbon interaction plays a fundamental role governing the kinetics of SWNT nucleation (and growth[36,37]), a fact that will be a recurrent theme throughout this work. In the case of Trajectory $Ni_{77}C_{39}$@1400K-5, Figure 2a shows that, by 96.08 ps, these polyyne chains themselves coalesced further, with very little "free carbon" remaining on the catalyst surface. In particular, the existence of a Y-shaped junction between two such polyyne chains at 96.08 ps was prominent. In this case, this branched polyyne chain was bound so weakly to the Ni-catalyst surface that, on occasions, it floated away from the surface itself, anchored to the surface only by two C−Ni bonds. Following the formation of this Y-junction, the "moment of

(29) Moors, M.; Amara, H.; Visart de Bocarme, T.; Bichara, C.; Ducastelle, F.; Kruse, N.; Charlier, J.-C. *ACS Nano* **2009**, *3*, 511–516.
(30) Lindemann, F. A. *Phys. Z.* **1910**, *11*, 609.
(31) Zheng, G.; et al. *J. Chem. Theor. Comput.* **2007**, *3*, 1349.
(32) Weinert, M.; Davenport, J. W. *Phys. Rev. B* **1992**, *45*, 13709.
(33) Wentzcovitch, R. M.; Martins, J. L.; Allen, P. B. *Phys. Rev. B* **1992**, *45*, 11372.
(34) Swope, W. C.; Andersen, H. C.; Berens, P. H.; Wilson, K. R. *J. Chem. Phys.* **1982**, *76*, 637–649.
(35) Martyna, G. J.; Klein, M. L.; Tuckerman, M. *J. Chem. Phys.* **1992**, *97*, 2635.
(36) Page, A. J.; Minami, S.; Ohta, Y.; Irle, S.; Morokuma, K. *Carbon* **2010**, *48*, 3014–3026.
(37) Ding, F.; Larsson, P.; Larsson, J. A.; Ahuja, R.; Duan, H.; Rosen, A.; Bolton, K. *Nano Lett.* **2007**, *8*, 463–468.

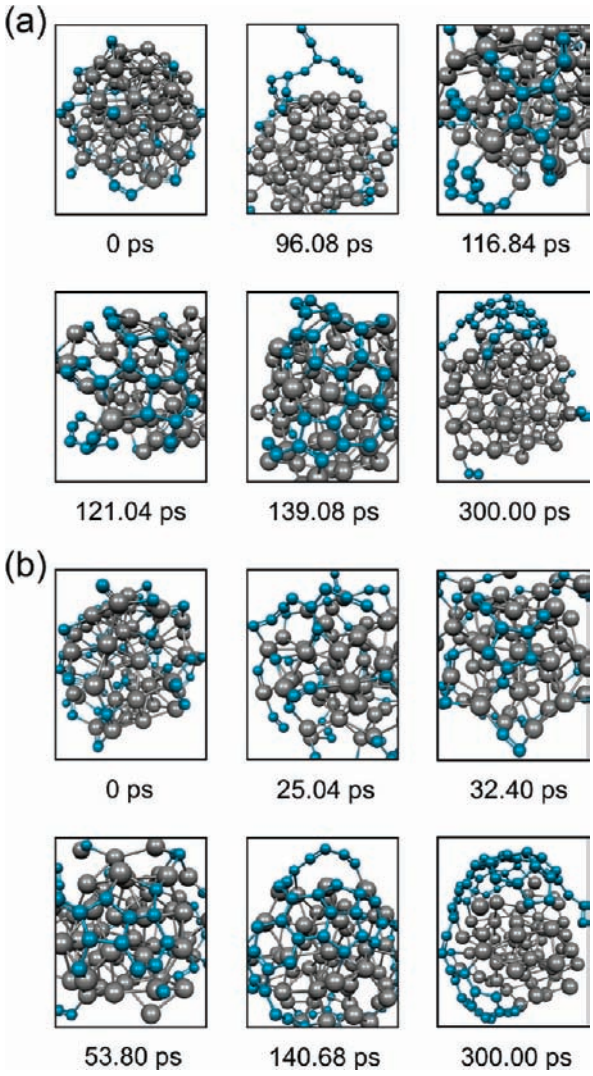

Figure 2. Evolution of SCC-DFTB/MD simulations of SWNT nucleation at 1400 K from Ni_xC_y nanoparticle precursors. (a) Trajectory $Ni_{77}C_{59}$@1400K-5 and (b) Trajectory $Ni_{58}C_{58}$@1400K-3. Color conventions as in Figure 1. Snapshot times given with respect to the beginning of the simulation.

nucleation" was observed when the polyyne "arms" formed a C−C bond between them due to their individual vibrational motions on the catalyst surface. This resulted in the formation of a five-membered ring at 116.84 ps. The continued vibrational motions of these shortened polyyne arms resulted in subsequent ring condensation, which over the subsequent 185 ps of simulation yielded a cap structure bound to the catalyst surface. From Figure 2b, which summarizes the SWNT nucleation mechanism observed in Trajectory $Ni_{58}C_{58}$@1400K-3, it is evident that a Y-shaped junction between two adjacent polyyne chains formed on the catalyst surface after 25.04 ps. The formation of the Y-shaped junction in Trajectory $Ni_{58}C_{58}$@1400K-3 was noticeably faster than that for Trajectory $Ni_{77}C_{39}$@1400K-5, assumedly due to the higher carbon concentration on the Ni surface. Nevertheless, the formation of this structural feature in Trajectory $Ni_{58}C_{58}$@1400K-3 occurred *via* an identical mechanism to that observed in Trajectory $Ni_{77}C_{39}$@1400K-5. It is also evident from Figure 2b that, following the formation of this Y-shaped junction, a five-membered ring was formed on the Ni surface at 32.40 ps, after which subsequent ring condensation yielded a SWNT cap precursor on the catalyst surface within 300 ps. Once again, this mirrored exactly the mechanism observed in Trajectory $Ni_{77}C_{39}$@1400K-5. However, the time necessary for the formation of the SWNT cap in Trajectory $Ni_{58}C_{58}$@1400K-3 was significantly less than that required in Trajectory $Ni_{77}C_{39}$@1400K-5. Identical mechanisms were also observed for SWNT nucleation from Ni_xC_y nanoparticle precursors at 800 and 2000 K (see Supporting Information).

It is therefore concluded that *the mechanism of SWNT nucleation from Ni_xC_y nanoparticle precursors is independent of temperature (between 800 and 2000 K) and the carbon concentration in the metal-carbide phase*. With respect to SWNT nucleation from $Ni_{39}C_{77}$ nanoparticle precursors, it was observed in most cases that constant temperature annealing ultimately culminated in the "death of the catalyst". That is, much of the catalyst surface being covered by the established sp^2-hybridized carbon network within the first 300 ps of simulation. In reality, such a catalyst would not be amenable to further decomposition of carbon feedstock species. It is noted here that these SWNT nucleation mechanisms reported in this work are identical to that we recently reported also using SCC-DFTB/MD simulations.[20] In the latter case however, an Fe_{38} catalyst was employed, onto which C_2 moieties were deposited before the complex was annealed at constant temperature. Thus, it is also concluded that *the mechanism of SWNT nucleation is independent of the origin of the carbon feedstock species and the metal catalyst employed*. Interestingly, it has recently been reported[38] that, in the case of continued SWNT growth, the opposite is in fact the case regarding the metal catalyst. That is, there is a distinct dependence of the SWNT growth mechanism on the type of catalyst employed, which is driven at the most fundamental level by the strength of the carbon−catalyst interaction itself.

In the case of SWNT nucleation from Ni_xC_y nanoparticle precursors, SWNT nucleation was initiated by the formation of a single five-membered ring. Subsequent ring condensation then occurred in a seemingly random fashion. Nonetheless, the populations of five- and six-membered rings exhibited a distinct dependence on the simulation temperature. This is evident from Figure 3, which shows these ring populations between 0 and 300 ps. Explicitly, the total numbers of five-, six-, and seven-membered rings formed at 1400 and 2000 K are noticeably higher than those at 800 K. This reflects the overall exothermicity of the SWNT nucleation process, which, in a thermodynamic sense, essentially amounts to the repeated formation of C−C bonds. However, seven-membered ring formation during SWNT nucleation was limited and is considered to be unimportant in the present context. Figure 3b shows that, at 1400 K, five-membered rings, instead of six- and seven-membered rings, were preferentially formed during the SWNT nucleation process. This was also the case at 800 K (Figure 3a), although ring formation in this case was itself limited. However, such preferential formation was not observed at 2000 K (Figure 3c). At this higher temperature, the numbers of five- and six-membered rings were essentially equal throughout the SWNT nucleation simulation. This difference is attributed directly to the influence of temperature on the dynamics of the nascent polyyne chains bound to the catalyst surface. In particular, at higher temperatures these polyyne chains exhibited greater translational and vibrational mobility on the catalyst surface. The probability of bond formation between third carbon

(38) Page, A. J.; Irle, S.; Morokuma, K. *J. Phys. Chem. C* **2010**, *114*, 8206–8211.

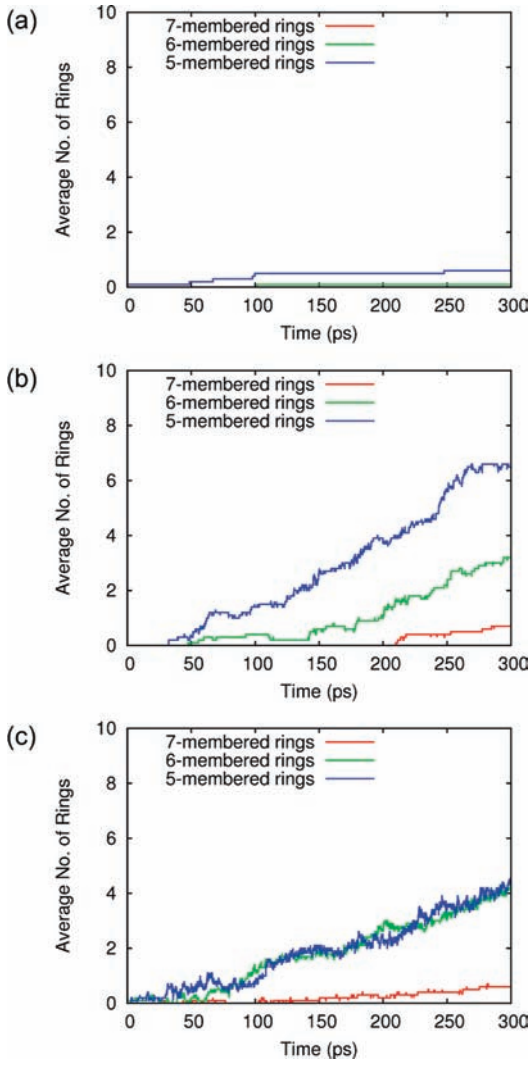

Figure 3. Dependence of SWNT nucleation from $Ni_{58}C_{58}$ on temperature: populations of five-, six-, and seven-membered rings at (a) 800, (b) 1400, and (c) 2000 K. All data averaged over 10 trajectories.

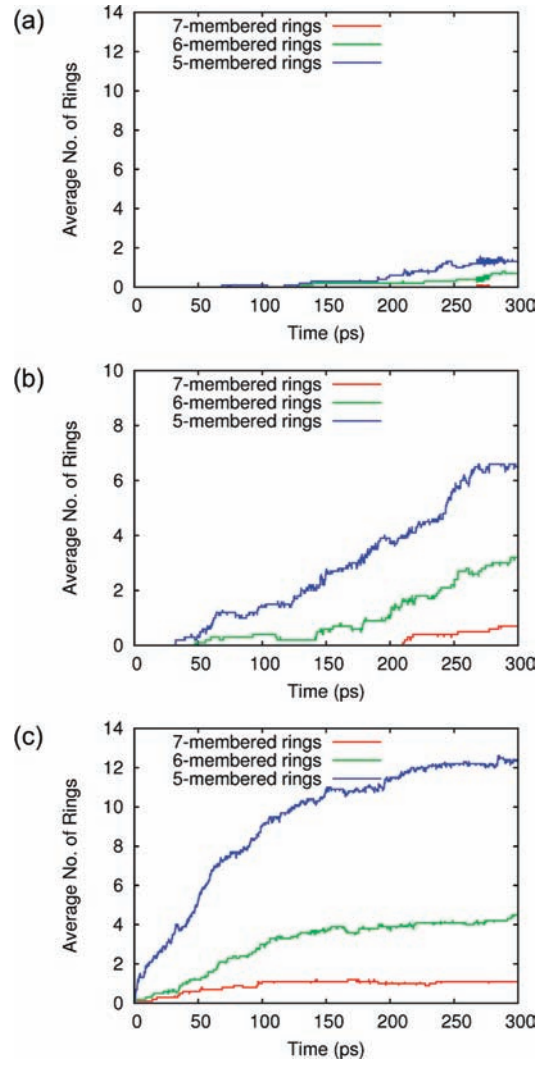

Figure 4. Dependence of SWNT nucleation from Ni_xC_y on carbon concentration at 1400 K: populations of five-, six-, and seven-membered rings from (a) $Ni_{77}C_{39}$, (b) $Ni_{58}C_{58}$, and (c) $Ni_{39}C_{77}$. All data averaged over 10 trajectories.

atoms (with respect to the polyyne Y-shaped junction) and hence six-membered ring formation was therefore increased.

The dependence of the SWNT nucleation process from Ni_xC_y nanoparticles on the initial carbon concentration is considered in Figure 4. In essence, this amounts to the dependence of the SWNT nucleation process on the size of the Ni catalyst particle, due to the speed at which the Ni−C phase separated. A distinct dependence of the ratio of five- and six-membered rings on the size of the Ni catalyst particle is evident from Figure 4. For $Ni_{77}C_{39}$ the average populations of five- and six-membered rings, shown in Figure 4a, are approximately equal after 300 ps of simulations, exhibiting a ratio of 1:0.54 (indeed this is also the case for the majority of the simulation up to 300 ps). However, upon increasing the carbon concentration (thus decreasing the size of the Ni catalyst particle), the average number of five-membered rings formed during the SWNT nucleation process increased substantially, compared to the average number of six-membered rings. Explicitly, SWNT nucleation from $Ni_{58}C_{58}$ at 1400 K featured a five- and six-membered ring ratio of 1:0.47 (Figure 4b), whereas SWNT nucleation from $Ni_{39}C_{77}$ at 1400 K featured a five- and six-membered ring ratio of 1:0.37 (Figure 4c). It has been established previously[20,39] that the most favorable ring structure formed on a highly convex catalyst surface is one consisting of five carbon atoms. Thus, the trends observed here correlate exactly with the relative curvatures of the Ni_{39}, Ni_{58}, and Ni_{77} surfaces. This same trend was also observed at 800 K (see Supporting Information). However, in this case the comparison was relatively limited, as there was very little ring condensation from $Ni_{77}C_{39}$ and $Ni_{58}C_{58}$ observed. Appreciable ring condensation was only observed by annealing $Ni_{39}C_{77}$ nanoparticles at this lower temperature. At 2000 K the populations of five- and six-membered rings during SWNT nucleation from $Ni_{77}C_{39}$ and $Ni_{58}C_{58}$ were approximately equal throughout the first 300 ps (see Supporting Information). However, during SWNT nucleation from $Ni_{39}C_{77}$, the number of six-membered rings formed on the catalyst surface actually exceeded the number of six-membered rings formed after *ca.* 30 ps of simulation. While this is contrary to the trends observed at 800 and 1400 K, it is not entirely unexpected, considering the relative thermodynamic stabilities of five- and six-membered

(39) Fan, X.; Buczko, R.; Puretzky, A. A.; Geohegan, D. B.; Howe, J. Y.; Pantelides, S. T.; Pennycook, S. J. *Phys. Rev. Lett.* **2003**, *90*, 145501.

rings in the nascent sp^2-hybridized carbon network at high temperature. Essentially, the higher temperature frequently facilitated the rearrangement of this growing network (i.e., by allowing the continual breaking and reformation of C−C bonds) and ultimately lead to the conversion of five-membered rings into six-membered rings.

3.2. Comparison of SWNT Nucleation from Fe_xC_y and Ni_xC_y Nanoparticles. We now consider the SWNT nucleation process from Fe_xC_y nanoparticle precursors. The independence of the SWNT nucleation mechanism from Ni_xC_y on several pertinent factors (*i.e.*, the origin of carbon feedstock, temperature, and initial carbon concentration) has been established in the preceding discussion. It is reasonable therefore to anticipate that SWNT nucleation from amorphous Fe_xC_y nanoparticles should proceed along an entirely predictable path. While this will be shown to be, in some sense, the case, certain marked differences between the dynamics/kinetics of SWNT nucleation from Fe_xC_y and Ni_xC_y nanoparticle precursors have been observed in our simulations. These differences will be the focus of the subsequent section.

To facilitate the direct comparison between Fe- and Ni-catalyzed SWNT nucleation, the SCC-DFTB/MD annealing of $Fe_{77}C_{39}$ and $Fe_{58}C_{58}$ nanoparticles at 1400 K is discussed presently. Snapshots of Trajectories $Fe_{58}C_{58}$@1400K-9 and $Fe_{39}C_{77}$@1400K-9, which typify the dynamics observed for these model systems, are presented in Figure 5. The populations of five-, six-, and seven-membered rings, averaged over 10 trajectories, observed during the annealing of $Fe_{77}C_{39}$, $Fe_{58}C_{58}$ and $Fe_{39}C_{77}$ are shown in Figure 6. From Figure 6 it is immediate that (according to these SCC-DFTB/MD simulations) the kinetics of SWNT nucleation from Fe_xC_y nanoparticles are of a fundamentally different nature, compared to that from Ni_xC_y nanoparticles. This is particularly the case with respect to lower concentrations of carbon in the nanoparticle precursor. For instance, Figures 5a and 6b both illustrate that SWNT nucleation from Fe_xC_y is significantly impeded, compared to their Ni_xC_y analogues. In particular, no five-, six-, or seven-membered rings were observed to *persist* in any of the $Fe_{77}C_{39}$ or $Fe_{58}C_{58}$ trajectories computed in this work. The formation of the polyyne Y-junction (the initial stage of the nucleation process) was also impeded in these cases. These two points are illustrated in Figure 5a and b and the movie in the Supporting Information corresponding to Trajectory $Fe_{58}C_{58}$@2000K-5. For instance, it was observed in Trajectory $Fe_{58}C_{58}$@1400K-9 that by 240 ps several polyyne chains had formed on the Fe surface. As shown in Figure 5a, at *ca*. 246.8 ps, two adjacent polyyne chains combined due to translational diffusion across the catalyst surface, forming a polyyne Y-junction. However, this was only a fleeting structure, as it was broken apart only *ca*. 6 ps after it was formed. In this case, the polyyne Y-junction was broken by the diffusion of surface metal atoms and the persistence of the terminal C−Fe bonds between the polyyne and the surface itself. Thus, the surface catalyst atoms were actively involved in this respect. From inspection of several other trajectories, this seems to be a typical feature of the impedance of SWNT nucleation from Fe_xC_y nanoparticles. Similarly, Figure 5b depicts the formation and subsequent destruction of a five-membered ring (following the formation of a polyyne Y-junction) on the catalyst surface. Although this five-membered ring was slightly more stable than the previously discussed polyyne Y-junction (lasting for *ca*. 9 ps), its fate was ultimately the same.

Consequently, a well-defined cap structure bound to the Fe catalyst surface after 300 ps of simulation was never observed

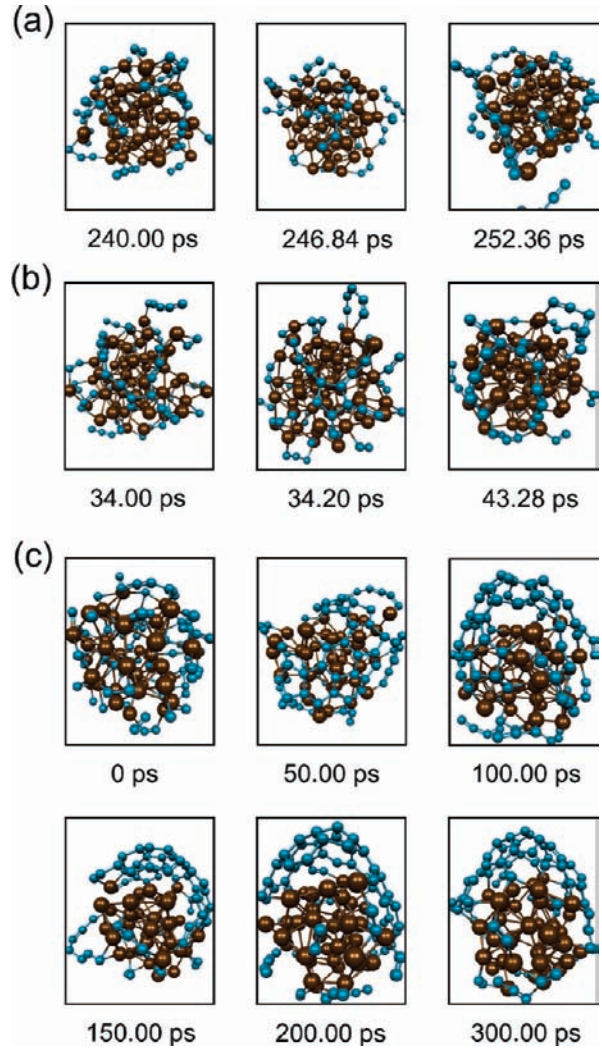

Figure 5. (a) Polyyne Y-junction formation and destruction during SWNT nucleation at 1400 K from $Fe_{58}C_{58}$ nanoparticle (Trajectory $Fe_{58}C_{58}$@1400K-9). (b) Five-membered ring formation and destruction during SWNT nucleation at 1400 K from $Fe_{58}C_{58}$ nanoparticle (Trajectory $Fe_{58}C_{58}$@1400K-9). (c) Evolution of SWNT nucleation at 1400 K from $Fe_{39}C_{77}$ nanoparticle (Trajectory $Fe_{39}C_{77}$@1400K-9). Cyan and brown spheres represent carbon and iron atoms, respectively. Snapshot times given with respect to the beginning of the simulation.

in any $Fe_{77}C_{39}$ or $Fe_{58}C_{58}$ trajectory. Nor was a cap structure attained in any $Fe_{77}C_{39}$/$Fe_{58}C_{58}$ trajectory at either 800 or 2000 K (see Supporting Information). This is reflected in Figure 7, which describes the kinetics of SWNT nucleation from Ni_xC_y and Fe_xC_y nanoparticles at 800, 1400, and 2000 K in terms of the "nucleation time". "Nucleation time" is defined here as the amount of time required before the first *persistent* five-membered ring is formed (averaged over 10 trajectories). From Figure 7 it is evident that SWNT nucleation occurred rapidly at 800, 1400, and 2000 K for each Ni_xC_y nanoparticle employed, with all nucleation times being much smaller than 300 ps. On the other hand, the nucleation time for $Fe_{77}C_{39}$ and $Fe_{58}C_{58}$ nanoparticles at 800, 1400, and 2000 K exceeded 300 ps. However, Figures 5c and 6c indicate that, by annealing a $Fe_{39}C_{77}$ nanoparticle at 1400 K, an extended sp^2-hybridized carbon structure was formed within 300 ps. In fact, this structure is well established within only 100 ps. The scenario of SWNT nucleation from supersaturated metal carbides is useful from a mechanistic point of view. Its physical significance, however,

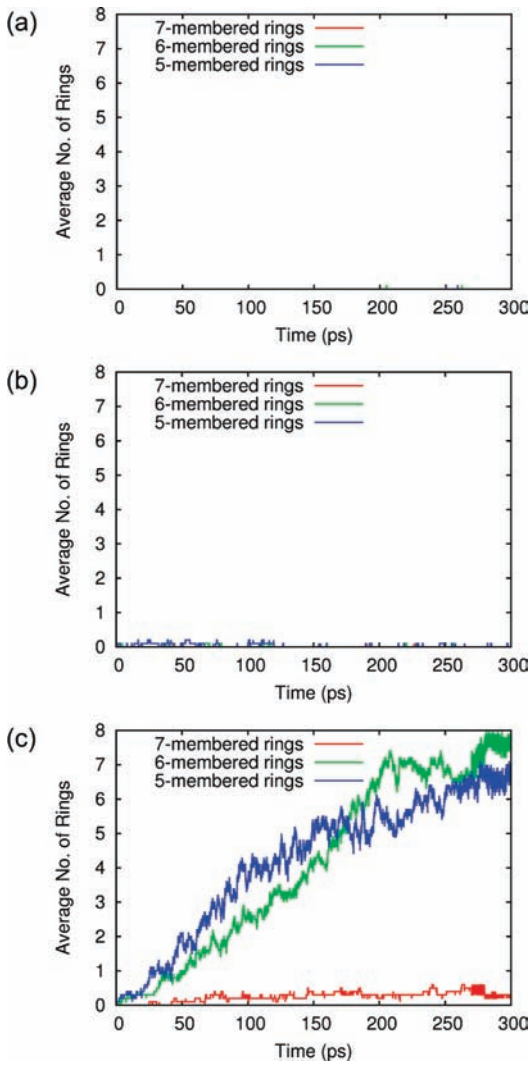

Figure 6. Dependence of SWNT nucleation from Fe_xC_y on carbon concentration at 1400 K: populations of five-, six-, and seven-membered rings from (a) $Fe_{77}C_{39}$, (b) $Fe_{58}C_{58}$, and (c) $Fe_{39}C_{77}$. All data averaged over 10 trajectories.

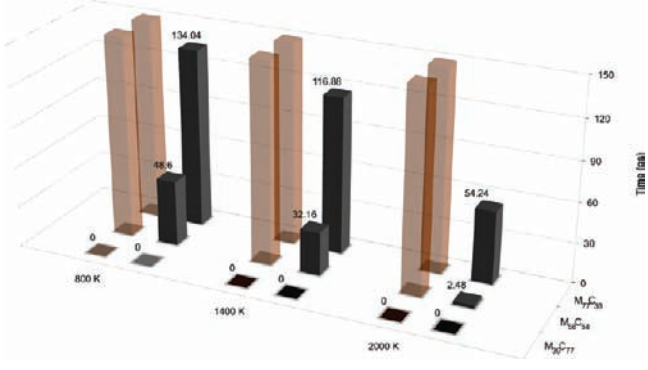

Figure 7. Average SWNT nucleation times (ps) from Ni_xC_y and Fe_xC_y nanoparticles at 800, 1400, and 2000 K. Gray and brown columns represent data for Ni_xC_y and Fe_xC_y, respectively. Transparent columns indicate an average SWNT nucleation time > 300 ps. All data averaged over 10 trajectories.

is limited in the present context, due to the size of the nanoparticle and the corresponding amount of carbon employed in this work. The SWNT nucleation mechanism observed in this case was identical to that observed during nucleation from Ni_xC_y nanoparticles and during nucleation from a $30C_2-Fe_{38}$ model complex,[20] as anticipated. Between 100 and 300 ps in Trajectory $Fe_{39}C_{77}$@1400K-9, a number of five-membered rings were converted to six-membered rings, further consolidating the nascent cap structure on the catalyst surface. This was observed to be a general phenomenon during the latter stages of SWNT nucleation for all $Fe_{39}C_{77}$ trajectories. This is evident from the average populations of five- and six-membered rings shown in Figure 6c. In the case of $Ni_{39}C_{77}$, the formation of an sp^2-hybidrized carbon structure generally brought about the catalytic deactivation of the Ni cluster, due to the partial/total encapsulation of the catalyst by the sp^2 structure itself. However, in the case of $Fe_{39}C_{77}$, this tendency toward encapsulation of the catalyst was much less pronounced compared to $Ni_{39}C_{77}$. In particular, the majority of $Fe_{39}C_{77}$ structures following 300 ps annealing at 800, 1400, and 2000 K (see Supporting Information) exhibited well-defined SWNT cap fragments bound to the catalyst surface after 300 ps of simulation, suggesting that SWNT nucleation from supersaturated iron-carbide nanoparticles is feasible.

Interestingly, even though SWNT nucleation from both Ni_xC_y and Fe_xC_y nanoparticles occurred *via* identical atomistic mechanisms, their ultimate outcomes differed, due to the differing influence of the catalyst on the self-rearrangement of the sp^2-hybridized carbon network itself. This influence arises from the relative strengths of the Ni−C and Fe−C interactions (with the latter being stronger than the former). Consequently, surface iron atoms exhibited a greater tendency toward "interfering" in the establishment of the sp^2-hybridized carbon network by repeatedly breaking newly formed C−C bonds, as illustrated in Figure 5a and b. This interference also assisted in the rearrangement of the sp^2-hybridized carbon network *via* the conversion of five-membered rings to six-membered rings, as illustrated in Figure 5c. Conversely, in the case of nickel, the metal−carbon interaction was weaker and so newly formed C−C bonds were more stable in a relative sense. This observation parallels the trends recently established regarding the influence of iron and nickel catalysts on continued SWNT growth.[36,38]

3.3. Dynamics of Carbon Precipitation from Fe_xC_y and Ni_xC_y Nanoparticles. The existence and stability of transition metal-carbide precursors (with respect to SWNT nucleation) is currently an outstanding issue among experimental and theoretical investigators alike. Indeed, the existence of "subsurface" iron and nickel carbide species (i.e., species featuring a bulk metal structure with carbon dissolved at and below the surface of the metal particle) has only recently been shown experimentally[19] and theoretically.[16,29] In this work, we have monitored the behavior of the Fe_xC_y and Ni_xC_y nanoparticle precursors during thermal annealing using SCC-DFTB/MD. Our aim in this regard is to investigate the persistence and stability of both the bulk and carbide/subsurface carbide species.

Figure 8 shows the "average carbon precipitation times" observed for Fe_xC_y and Ni_xC_y nanoparticles at 800, 1400, and 2000 K. "Average carbon precipitation time" is defined here as the time at which all carbon atoms originally within the iron/nickel bulk have migrated to reside on the iron/nickel surface. This has been achieved by monitoring the distance between each carbon atom and the center-of-mass of all metal atoms at each MD iteration of the simulation (Figure 8a). It is evident from Figure 8b that there are distinct differences in the behaviors of the Fe_xC_y and Ni_xC_y nanoparticle precursors employed in this work. For example, for a given carbon concentration, the average

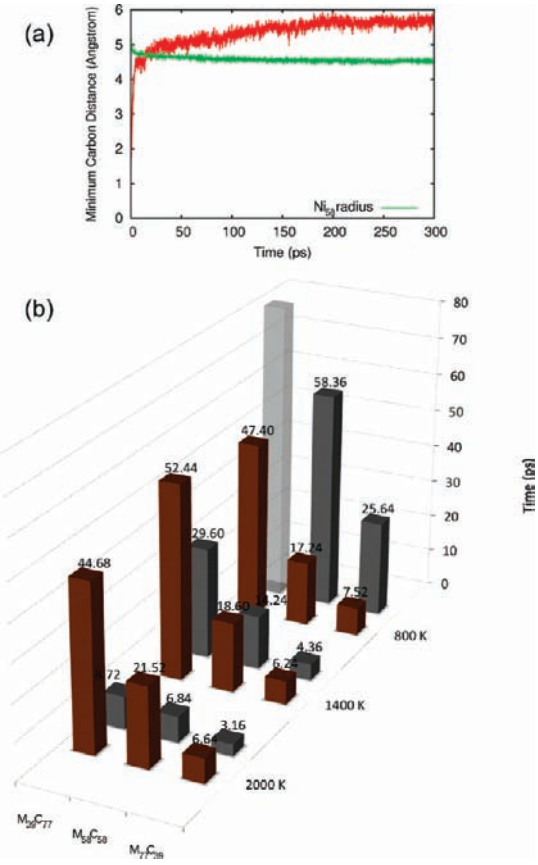

Figure 8. (a) Minimal distance (red) between all carbon atoms and Ni_{58} center of mass during SWNT nucleation from $Ni_{58}C_{58}$ nanoparticle. (b) Average carbon precipitation times (ps) from Ni_xC_y and Fe_xC_y nanoparticles at 800, 1400, and 2000 K. "Average carbon precipitation time" is defined as the first time at which the minimal distance in (a) is greater than the Ni_{58} radius. Gray and brown columns represent data for Ni_xC_y and Fe_xC_y, respectively. Transparent columns indicate an average carbon precipitation time > 300 ps. All data averaged over 10 trajectories.

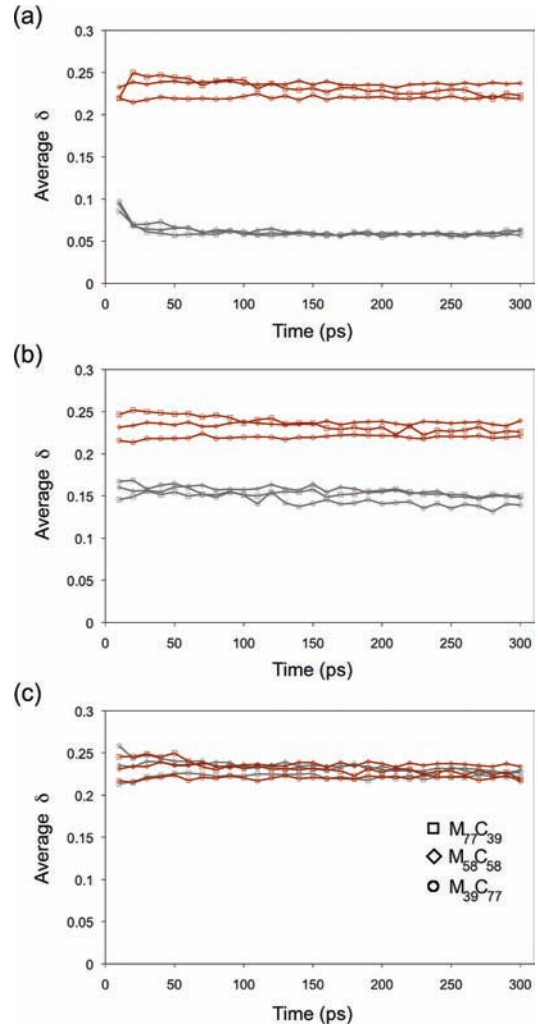

Figure 9. SCC-DFTB/MD δ values of M_xC_y nanoparticles at (a) 800, (b) 1400, and (c) 2000 K. All data averaged over 10 trajectories, at intervals of 10 ps. Brown and gray lines correspond to Fe_xC_y and Ni_xC_y data, respectively. $\delta = 0.1$ is the accepted threshold signifying the solid−liquid phase transition.

carbon precipitation time for Ni_xC_y was inversely related to simulation temperature. These nanoparticles also increased in stability with increasing carbon concentration. Most notably, the average carbon precipitation time observed for $Ni_{39}C_{77}$ at 800 K exceeded 300 ps. Figure 8b also indicates that Fe_xC_y nanoparticles also increased in stability (in terms of average carbon precipitation time) with increasing carbon concentration. However, the stabilities of Fe_xC_y nanoparticles were essentially independent of simulation temperature. At 1400 and 2000 K, the average precipitation times for Ni_xC_y nanoparticles were always less than those for the analogous Fe_xC_y nanoparticles, irrespective of carbon concentration. This suggests that the dynamics of carbon precipitation here may be explained with recourse to the relative strengths of the Ni−C and Fe−C interactions (that is, the carbon atoms within Fe_xC_y are held within the metal bulk more tightly, compared to the carbon atoms within Ni_xC_y). However, a single exception to this trend at 800 K is evident from Figure 8. At this temperature the average carbon precipitation times for Ni_xC_y were significantly higher than those for Fe_xC_y. This exception can be explained with recourse to the evolution of the phase of the metal nanoparticles, estimated by monitoring δ,[40] during the precipitation process (see Figure 9). It is immediate from this figure that the Ni_xC_y nanoparticles at 800 K are the only species of those considered in this work to exist in the solid phase (the commonly accepted value signifying the solid/liquid phase transition is $\delta = 0.1$[40]). Moreover, Figure 9 shows that the phase of Ni_xC_y is far more sensitive to the temperature range employed here, compared to Fe_xC_y. The latter exhibited no discernible shift in δ whatsoever across this temperature range, residing in the liquid phase at 800, 1400, and 2000 K. The relative dynamics of carbon precipitation from Fe_xC_y and Ni_xC_y nanoparticles are therefore governed by the interplay of two factors, viz. the strength of the metal−carbon interaction and the phase of the nanoparticle itself. This conclusion complements those made in a recent theoretical investigation[41] concerning the effect of the interplay between dynamic-coexistence melting and surface melting on carbon diffusion in Ni nanoparticles. Moreover, it is evident that the phase of the nanoparticle dominated these dynamics at lower temperatures, whereas the strength of the metal−carbon interaction became dominant at higher temperatures. At intermediate temperature, the competition between these two factors yielded more equivalent average carbon precipitation times.

(40) Zhou, Y.; Karplus, M.; Ball, K. D.; Berry, R. S. *J. Chem. Phys.* **2002**, *116*, 2323–2329.

(41) Neyts, E. C.; Bogaerts, A. *J. Phys. Chem. C* **2009**, *113*, 2771–2776.

From consideration of Figure 8 however, it is arguable that the strength of the metal−carbon interaction is slightly more influential than the nanoparticle phase at 1400 K.

It is also noted at this point that rapid precipitation of carbon from the nanoparticle bulk to the nanoparticle surface did not necessarily result in rapid SWNT nucleation. Instead, an intermediate stage prior to SWNT nucleation was observed. The structure formed in the intervening period was essentially a surface (or subsurface) carbide, i.e. Fe_xC_y/Ni_xC_y nanoparticles in which all carbon density was located on or near the surface of the metal. The existence of this intermediate stage can be inferred from comparison of Figures 7 and 8. Comparison of these figures also shows that the stability of the surface/subsurface carbide intermediate structure was most prominent for Fe_xC_y catalysts. For instance, Figure 8 shows that annealing Fe_xC_y at 800, 1400, and 2000 K yielded a segregated Fe−C complex (with all carbon density located at the catalyst surface) almost immediately. Nevertheless, the time required for the formation of a SWNT cap structure exceeded 300 ps (Figure 7) in most cases (the exception here is $Fe_{39}C_{77}$, due to the unrealistically large amount of carbon "dissolved" in the nanoparticle precursor). This is consistent with the trends discussed previously regarding the kinetics of SWNT nucleation on Fe_xC_y nanoparticles and is the result of the same phenomenon, *viz*. the relative strengths of the Fe−C and Ni−C interactions. These results also complement recent experimental and theoretical investigations into the subsurface carbide phenomenon on Fe and Ni catalysts.[16,19,21,29] It is concluded then that SWNT nucleation from these metal-carbide nanoparticles consists of three distinct stages, *viz*. precipitation of carbon from the nanoparticle bulk, formation of a surface/subsurface carbide, and finally the establishment of the sp^2 network constituting the SWNT cap structure. However, while the first of these processes is dictated by the interplay of the phase of the nanoparticle and the strength of the metal−carbon interaction, the second and third stages of this process are governed only by the strength of the metal−carbon interaction.

4. Conclusion

SWNT nucleation from Fe_xC_y and Ni_xC_y nanoparticle precursors has been simulated using SCC-DFTB/MD. In all cases considered in this work, SWNT nucleation occurred *via* three distinct stages, viz. the precipitation of carbon from the carbide nanoparticle bulk, the formation of a surface/subsurface carbide species, and the formation of a nascent sp^2-hybridized carbon cap structure. SWNT nucleation from Fe_xC_y and Ni_xC_y nanoparticles ultimately exhibited striking similarities and differences. For example, the SCC-DFTB/MD simulations presented in this work indicated that the atomistic mechanism of SWNT nucleation was invariant with respect to several pertinent factors. In all cases of carbon concentration and temperature considered here, no change in the SWNT nucleation mechanism itself was observed. SWNT nucleation followed the formation of polyyne chains and their subsequent coalescence on the transition metal catalyst surface. On the other hand, the kinetics of SWNT nucleation exhibited distinct dependences on these same factors (i.e., carbon concentration and temperature). The simulations presented in this work indicate that SWNT nucleation from Ni_xC_y nanoparticles proceeded more favorably compared to nucleation from Fe_xC_y nanoparticles. This observation was consistent with both experimental and theoretical conclusions of SWNT growth rates.[36,38,42] Interestingly, although SWNT nucleation from Fe_xC_y and Ni_xC_y nanoparticle precursors took place by an identical route, the ultimate outcomes of these processes differed substantially. These differences in SWNT nucleation kinetics were attributed directly to the relative strengths of the metal−carbon interaction. The strength of the metal−carbon interaction was also observed to play a dominant role in dictating the precipitation of carbon from the nanoparticle bulk and the longevity of the resultant surface/subsurface carbide species. The stability of the metal-carbide bulk, however, was determined by the interplay of this metal−carbon interaction strength and the phase of the nanoparticle itself. Nevertheless, in both iron and nickel cases, the initially carbon-rich carbide particles rapidly lost their carbon content, with this carbon being drawn out from the metal phase as soon as a surface carbon structure began to nucleate. This finding is in accord with the traditional VLS mechanism of SWNT formation.[4,7]

Acknowledgment. This work was in part supported by a CREST (Core Research for Evolutional Science and Technology) grant in the Area of High Performance Computing for Multiscale and Multiphysics Phenomena from the Japanese Science and Technology Agency (JST). One of the authors (S.I.) also acknowledges support by the Program for Improvement of Research Environment for Young Researchers from Special Coordination Funds for Promoting Science and Technology (SCF) commissioned by the Ministry of Education, Culture, Sports, Science and Technology (MEXT) of Japan. Simulations were performed using the computer resources at the Academic Center for Computing and Media Studies (ACCMS) at Kyoto University as well as at the Research Center for Computational Science (RCCS) at the Institute for Molecular Science (IMS).

Supporting Information Available: Structures of Ni_xC_y nanoparticles following 300 ps annealing at 800 and 2000 K; SWNT nucleation mechanisms from Ni_xC_y nanoparticles at 800 and 2000 K; average ring populations observed during SWNT nucleation from Ni_xC_y nanoparticles at 800 and 2000 K; QuickTime movie showing Trajectory $Fe_{58}C_{58}$@2000K-5 (Fe-catalyzed SWNT nucleation); structures of Fe_xC_y nanoparticles following 300 ps annealing at 800 and 2000 K; and average ring populations observed during SWNT nucleation from Ni_xC_y nanoparticles at 800, 1400, and 2000 K. This material is available free of charge via the Internet at http://pubs.acs.org.

JA106264Q

(42) Mora, E.; Harutyunyan, A. R. *J. Phys. Chem. C* **2008**, *112*, 4805–4812.